

Chord: Chain of Rendering Decomposition for PBR Material Estimation from Generated Texture Images

ZHI YING*, Ubisoft La Forge, China

BOXIANG RONG*, ETH Zürich, Switzerland

JINGYU WANG, ETH Zürich, Switzerland

MAOYUAN XU, Ubisoft La Forge, China



Fig. 1. **PBR materials generated by our method.** Keywords in the text prompts used for generating each material (from left to right) are: *fabric with flower embroidery*, *cobblestone*, *green marble*, *salmon fish meat*, *wood floor*, *colorful stone wall*, *cyberpunk iron wall*, and *wet mossy rock*.

Material creation and reconstruction are crucial for appearance modeling but traditionally require significant time and expertise from artists. While recent methods leverage visual foundation models to synthesize PBR materials from user-provided inputs, they often fall short in quality, flexibility, and user control. We propose a novel two-stage generate-and-estimate framework for PBR material generation. In the generation stage, a fine-tuned diffusion model synthesizes shaded, tileable texture images aligned with user input. In the estimation stage, we introduce a chained decomposition scheme that sequentially predicts SVBRDF channels by passing previously extracted representation as input into a single-step image-conditional diffusion model. Our method is efficient, high quality, and enables flexible user control. We evaluate our approach against existing material generation and estimation methods, demonstrating superior performance. Our material estimation method shows strong robustness on both generated textures and in-the-wild photographs. Furthermore, we highlight the flexibility of our framework across diverse applications, including text-to-material, image-to-material, structure-guided generation, and material editing.

CCS Concepts: • **Computing methodologies** → **Appearance and texture representations**.

Additional Key Words and Phrases: Appearance Modeling, Material Generation, Texture Synthesis, SVBRDF, Image-conditional Diffusion Models

*Both authors contributed equally to the paper

Authors' Contact Information: Zhi Ying, zhi.ying@ubisoft.com, Ubisoft La Forge, Shanghai, China; Boxiang Rong, borong@student.ethz.ch, ETH Zürich, Zürich, Switzerland; Jingyu Wang, jingyuwang@student.ethz.ch, ETH Zürich, Zürich, Switzerland; Maoyuan Xu, mao-yuan.xu@ubisoft.com, Ubisoft La Forge, Chengdu, China.

1 Introduction

Generating materials that represent the appearance of objects has been a long-standing focus in the computer graphics communities. Early methods primarily synthesized RGB textures. With the rise of physically based rendering (PBR) workflows, materials are now commonly represented as spatially-varying bidirectional reflectance distribution functions (SVBRDFs). This advancement allows for more realistic representations of surface properties like reflectance and roughness but significantly increases complexity. The generation process now must handle multiple channels (e.g., basecolor, normal, roughness, and metalness maps) while ensuring precise spatial alignment. We treat these channels as distinct modalities due to their differing physical meanings. A visualization of their data distribution is shown in Fig. 2.

Recent work aims to simplify this process by compressing multiple channels into one latent space, and leverage specialized generative models [Vecchio et al. 2024a,b; Zhou et al. 2022] to generate materials with certain level of user control. However, the flexibility and quality remains limited due to the constraints of their coupled architectures.

To address this challenge, we propose a two-stage *generate-and-estimate* framework that enables flexible user control. The first stage leverages a generative model, guided by various control techniques, to generate texture RGB images aligned with user inputs. The second stage employs our novel *chain-of-rendering-decomposition* (Chord) pipeline to predict SVBRDF channels through sequential steps.

Texture Generation involves creating tileable texture RGB images that represent top-down views of materials. Traditional example-based methods generate textures that are visually similar to user-provided exemplars [Wei et al. 2009]. While effective, they are often limited by the quality of input examples and can produce only a narrow range of variations. More recently, text-to-image generative models have been applied to texture generation [Chen et al. 2023], showing greater flexibility and promising results. Additionally, the controllability of these models can be enhanced through additional input conditions, such as line art and depth maps [Zhang et al. 2023]. Building on this approach, we employ a fine-tuned version of SDXL [Podell et al. 2024] for generating texture RGB images. Our model is trained on texture images rendered under predefined lighting and camera conditions, with each image paired with a descriptive caption. To enable the tileability of the generated images, we use circular padding for all the convolutional layers.

Material estimation focuses on inverse rendering, where shaded images of certain materials are used to estimate its SVBRDF channels. This task is inherently challenging due to its under-constrained nature. Recent intrinsic decomposition approaches [Kocsis et al. 2024; Zeng et al. 2024] attempt to address this challenge by leveraging visual foundation models fine-tuned on modality-specific data, and use their strong prior knowledge to reduce the uncertainties. These data-driven methods require large amounts of training data and significant time to generalize effectively to novel materials. Moreover, they ignore the intrinsic relationships between different channels, often failing to accurately recover the expected material appearance.

Therefore, to preserve the intrinsic relationships among SVBRDF channels, we propose a novel chained scheme for image-conditional dense prediction diffusion models, where channels are predicted sequentially by conditioning on previously extracted representation. Our specific chain design named Chord is derived from the rendering equation of PBR materials, which predicts basecolor first, followed by normals with height, and finally roughness and metalness. The decomposition task is simplified by leveraging the implicitly predefined lighting and camera conditions between the two stages. To mitigate interference between different combinations of input and output modalities, we replace several U-Net blocks with a modular conditioning mechanism, termed *LEGO-conditioning*.

During training, our chained scheme relies on clean intermediate representations, differing from standard diffusion training, which uses noisy samples. To address this, we adopt the single-step approach from [Garcia et al. 2024; He et al. 2024], which not only ensures deterministic outputs but also improves inference efficiency by eliminating the need for multi-step denoising. Representative examples of generated PBR materials are shown in Fig. 1.

In summary, our main contributions are:

- A two-stage generate-and-estimate framework that enables flexible user control and simplifies material estimation via implicitly shared lighting and camera conditions.
- A chained scheme for multi-modal dense prediction using image-conditional diffusion model to capture inter-modal dependencies.
- The proposed Chord pipeline, which explicitly models the intrinsic relationships among SVBRDF modalities, combining

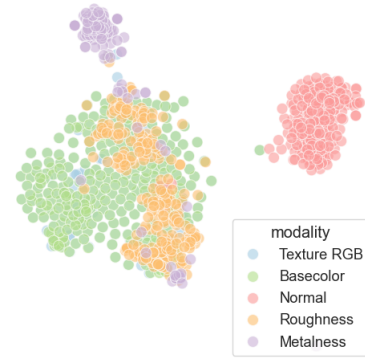


Fig. 2. **2D t-SNE visualization of latent vectors.** Texture RGB and basecolor modalities exhibit significant overlap, suggesting a strong bijective relationship. The normal modality forms a distinct cluster. Metalness vectors are concentrated near binary values (0 and 1), while roughness vectors are more evenly distributed across the (0, 1) range.

LEGO-conditioning and single-step fine-tuning for efficient, high-quality material estimation.

2 Related Work

Material Estimation. The methods introduced by Aittala et al. [Aittala et al. 2015; Miika Aittala 2016] aim to reduce the number of input images required for material estimation by assuming a fixed, centrally positioned point light source for illumination. These are the first optimization-based methods for few-shot material estimation. However, they rely heavily on hand-crafted heuristics and empirical priors. Deschaintre et al. [Deschaintre et al. 2018] introduce the first large synthetic dataset for material estimation and use a variation of U-Net [Ronneberger et al. 2015] to predict SVBRDF channels. Subsequent works [Gao et al. 2019; Li et al. 2017, 2018; Martin et al. 2022; Sartor and Peers 2023; Zhou and Kalantari 2022] follow similar data-driven approaches to estimate materials from single or multiple images. MATch [Shi et al. 2020] makes the procedural design of materials differentiable, enabling the optimization of procedural components from images. SurfaceNet [Vecchio et al. 2021] incorporates adversarial loss for unlabeled real-world images, while Material Palette [Lopes et al. 2024] adopts unsupervised domain adaptation to address the domain shift from synthetic training sets to real-world texture photos. Recently, a larger synthetic dataset, MatSynth [Vecchio and Deschaintre 2024], was released, further improving the performance of previous data-driven methods.

Material Synthesis. With the rise of generative models, they have become the most commonly used approaches for material generation. Earlier works [Guerrero et al. 2022; Zhao et al. 2020; Zhou et al. 2022, 2023] utilize auto-regressive models or GANs to generate stationary textures with material properties. With recent advancements in diffusion models [Ho et al. 2020; Rombach et al. 2021], more diffusion-based methods [Vecchio et al. 2024a,b; Xin et al. 2024] have emerged. Text2Mat [He et al. 2023] proposes a two-stage text-to-material pipeline, using a fine-tuned Stable Diffusion model to generate center-lit RGB exemplars, followed by an

image-to-image translation model to produce SVBRDF channels. ReflectanceFusion [Xue et al. 2024] adopts a similar pipeline, but employs a latent code as the intermediate representation between the two stages.

Material synthesis and estimation can be unified in a single framework. MaterialGAN [Guo et al. 2020] uses a GAN trained on a large synthetic dataset for material generation and performs material estimation by searching in the latent space. Henzler et al. [Henzler et al. 2021] train an image-to-image translation model with an encoder-decoder architecture, enabling both material generation and latent space sampling. MatFusion [Sartor and Peers 2023] and DiffMat [Yuan et al. 2024] adopt diffusion models and formulate material estimation as a conditioned generation task. MatFuse [Vecchio et al. 2024b] and ControlMat [Vecchio et al. 2024a] adapt Stable Diffusion models by modifying encoders and decoders to directly generate SVBRDF channels. MaterialPicker [Ma et al. 2025] adapt a Diffusion Transformer text-to-video model for material generation by treating material maps as video frames.

Intrinsic Decomposition. Our material estimation stage draws inspiration from intrinsic decomposition methods. Most current intrinsic decomposition models are trained on synthetic indoor datasets. Kocsis et al. [Kocsis et al. 2024] make diffusion models dependent on input images by concatenating them with noise in the latent space. RGB \leftrightarrow X [Zeng et al. 2024] leverages similar idea and uses keyword text to conditionally decompose intrinsic channels. Careaga and Aksoy [Careaga and Aksoy 2023, 2024] achieve high-quality decompositions on in-the-wild images using a step-by-step feed forward pipeline. Our method uses RGB \rightarrow X model of RGB \leftrightarrow X as backbone and improves its performance by single-step fine-tuning, the LEGO-conditioning and the Chord pipeline.

Image-conditional Dense Prediction Diffusion Models. Diffusion models [Ho et al. 2020; Rombach et al. 2021; Song et al. 2021], as visual foundation models, have shown great promise for various downstream tasks. Marigold [Ke et al. 2024] is the first to propose repurposing diffusion models for dense prediction tasks. It spatially conditions the diffusion model in a lightweight manner for depth estimation. Several subsequent works [Fu et al. 2024; Garcia et al. 2024; He et al. 2024; Lee et al. 2024; Xu et al. 2024] have improved upon this approach, with most focusing on single-modality predictions. Notably, some methods, such as GeoWizard [Fu et al. 2024], incorporate a switch to handle multiple modalities. Building on this foundation, our approach extends image-conditional dense prediction diffusion models to the multi-modal material domain, supporting four SVBRDF modalities.

3 Preliminaries

Latent Diffusion Models. LDMs such as Stable Diffusion (SD) [Rombach et al. 2021], operate in lower dimensional latent space to efficiently model the high dimensional data distribution, such as high resolution images. To facilitate transformation between data space and latent space, LDMs employ a pair of auto-encoders, $\{\mathcal{E}(\cdot), \mathcal{D}(\cdot)\}$ to reconstruct sample $\mathbf{x} \approx \mathcal{D}(\mathcal{E}(\mathbf{x}))$. In the latent space, LDMs incorporate a forward process and a reverse process. The forward process progressively destructs the data by injecting noise. For a

given time step $t \in [1, T]$, the forward process for the latent code \mathbf{z}_t can be written in closed form: $\mathbf{z}_t = \sqrt{\bar{\alpha}_t} \mathbf{z}_0 + \sqrt{1 - \bar{\alpha}_t} \epsilon$, where $\epsilon \sim \mathcal{N}(0, I)$, $\bar{\alpha}_t = \prod_{i=1}^t \alpha_i$, $\alpha_t = 1 - \beta_t$, and β_t is the noise schedule. Conversely, the reverse process gradually removes noise from its inputs by predicting \mathbf{z}_{t-1} given \mathbf{z}_t using a trained neural network. Specifically, in the v-prediction parametrization [Salimans and Ho 2022], the neural network \mathbf{v}_θ is trained to predict velocity $\hat{\mathbf{v}}_t$, and the corresponding loss at time step t is: $\mathcal{L}_\theta = \|\mathbf{v}_t - \mathbf{v}_\theta(\mathbf{z}_t, t)\|_2^2$, where $\mathbf{v}_t = \sqrt{\bar{\alpha}_t} \epsilon - \sqrt{1 - \bar{\alpha}_t} \mathbf{z}_0$.

Image-conditional Latent Diffusion Models. In addition to the latent code of the data sample $\mathbf{z}_0 = \mathcal{E}(\mathbf{x})$, an extra conditioning image \mathbf{I}_c and its latent code $\mathbf{c} = \mathcal{E}(\mathbf{I}_c)$ are provided. During training, noise is added only to \mathbf{z}_0 . To incorporate this additional conditioning input, the parameter size of the U-Net’s first convolutional layer, *Conv-In* denoted as ϕ is doubled. The model predicts velocity as $\hat{\mathbf{v}}_t = \mathbf{v}_\theta(\mathbf{c}, \mathbf{z}_t, t)$. By treating the two halves of the doubled Conv-In layer as independent feature encoders, the predicted velocity can be reformulated as:

$$\hat{\mathbf{v}}_t = \mathbf{v}_{\theta'}(\phi_1(\mathbf{c}) + \phi_2(\mathbf{z}_t), t) \quad (1)$$

where $\theta' = \theta \setminus (\phi_1 \cup \phi_2)$, ϕ_1 and ϕ_2 represent the two halves of the Conv-In. This formulation is easily extensible to multiple conditioning images, as elaborated in Section 4.2.1.

4 Method

Our framework follows a two-stage generation-and-estimation approach, as depicted in Fig. 3.

4.1 Texture RGB Generation

Our generation stage uses a fine-tuned SDXL diffusion model [Podell et al. 2024] to produce texture RGB images $I_{\text{RGB}} \in \mathbb{R}^{3 \times H \times W}$ from diverse inputs including text prompts, reference images, and other control signals. The model is trained on a custom dataset of PBR textures rendered under consistent top-down view and directional lighting using our differentiable renderer \mathcal{R} .

The renderer \mathcal{R} implements Cook-Torrance BRDF [Cook and Torrance 1982] with: (1) Trowbridge-Reitz GGX normal distribution [Trowbridge and Reitz 1975], (2) Schlick-GGX geometry term [Karis 2013], and (3) Schlick’s Fresnel approximation [Schlick 1994]. This same renderer is also used for material estimation and rendering loss computation in the next stage.

4.2 Material Estimation

Given the generated image I_{RGB} , our goal is to decompose the SVBRDF channels $\text{MAT} = \{b, n, h, r, m\}$, where b denotes basecolor, n normal, h height, r roughness, and m metalness. To train our material estimation model, we construct a dataset of paired samples $(\text{MAT}, I_{\mathcal{R}})$, where $I_{\mathcal{R}} = \mathcal{R}(\text{MAT}; l)$, l is a randomly rotated directional light. We assume that the rendering $I_{\mathcal{R}}$ should reproduce I_{RGB} under the same implicitly predefined lighting and camera conditions. This assumption holds in the majority of cases, see Fig. 9 and Fig. 10d for examples.

The training process for our material estimation model consists of two phases:

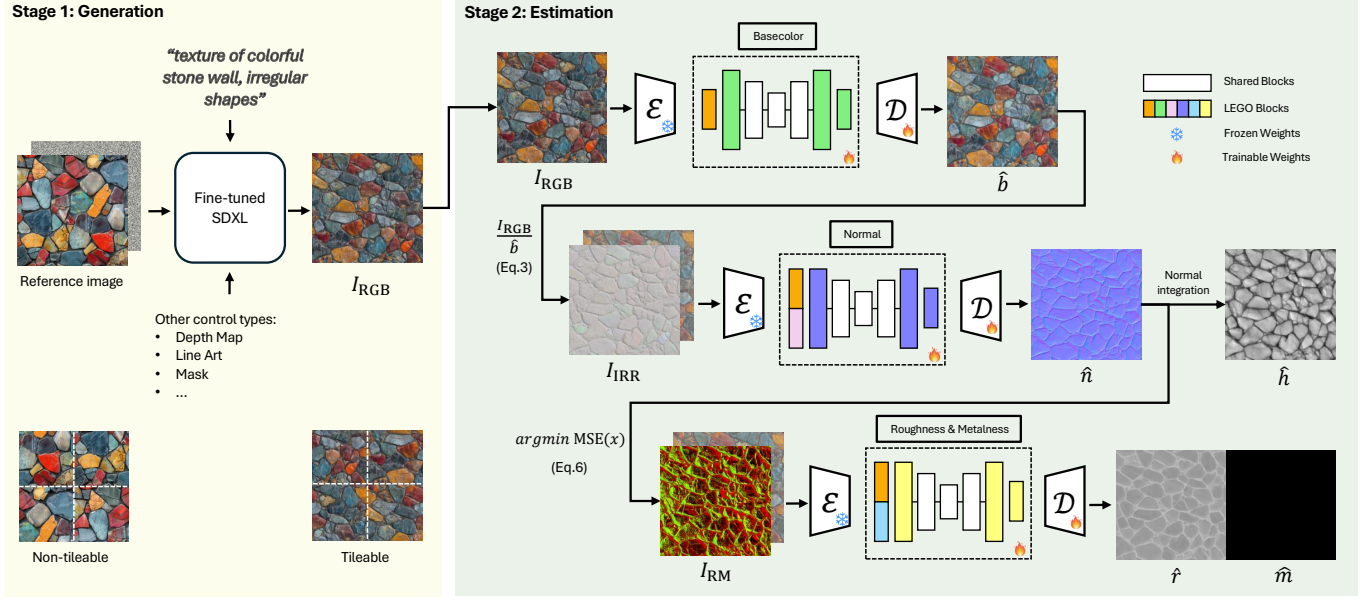


Fig. 3. **Method Overview.** **Stage 1:** Tileable texture image (I_{RGB}) generation using a fine-tuned diffusion model, controllable via user guidance (text prompts, reference images, or other control types). **Stage 2:** Material estimation predicts SVBRDF channels sequentially: (1) basecolor \hat{b} , (2) normal \hat{n} (with height \hat{h} derived via normal integration), and (3) roughness \hat{r} and metalness \hat{m} . Each step’s input is computed from previous outputs. LEGO-conditioning provides modality-specific weights while maintaining shared backbone weights for alignment. See Section 4.2 for details. Reference image from Vecteezy.

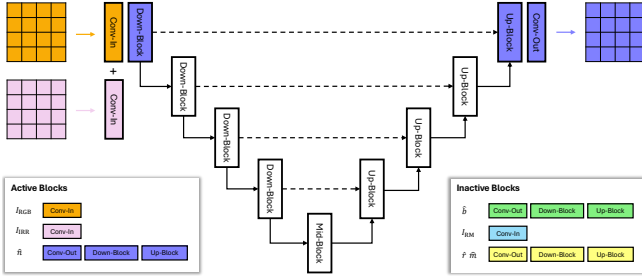


Fig. 4. **Detailed illustration of LEGO-conditioning.** Using the normal prediction step as an example, we illustrate the block-level architecture of the U-Net. We also highlight the corresponding active and inactive LEGO-conditioning blocks in this step.

- (1) **Pretraining Phase (optional)** – employs standard diffusion training to initialize and warm up the model weights.
- (2) **Single-step Phase** – serves as the primary training stage, utilizing the Chord pipeline along with image-space losses.

Below, we detail two key modifications to the image-conditional diffusion model: LEGO-conditioning and Chord pipeline.

4.2.1 LEGO-conditioning. Building on the $RGB \rightarrow X$ [Zeng et al. 2024], we employ CLIP text embeddings τ as target channel switches when predicting different modalities. However, as shown in our ablation study (Table 5), directly adapting a chained pipeline reveals weight conflicts between modalities in shared layers.

We address this with LEGO-conditioning, extending Eq.1 to support multiple conditions. The v-prediction becomes:

$$\hat{\mathbf{v}}_t = \mathbf{v}_{\theta'} \left(\frac{\sum_{i=1}^k \phi_i(\mathbf{c}_i) + \phi_z(\mathbf{z}_t)}{k+1}, \tau(D_z), t \right), \quad (2)$$

where \mathbf{c}_i are conditioning latents, \mathbf{z}_t is the noisy latent of the target channel, and D_z is its text description. The features are averaged to maintain consistent magnitude. Inspired by recent works [Hong et al. 2024; Liu et al. 2023] and based on the SD 2.1 architecture [Romach et al. 2021], we adopt separate first *Down-Block*, last *Up-Block*, and *Conv-Out* modules for each target channel, while sharing intermediate U-Net blocks to preserve spatial alignment. Details of the model architecture are shown in Fig. 4. This design achieves effective channel separation with minimal computational and memory overhead.

During the Pretraining Phase, the training objective minimizes the loss $\mathcal{L}_\theta = \|\mathbf{v}_t - \hat{\mathbf{v}}_t\|_2^2$, where $\mathbf{v}_t = \sqrt{\alpha_t}\epsilon - \sqrt{1 - \alpha_t}\mathbf{z}_0$. In the Single-step Phase, we set $t = T$, the \mathbf{z}_t term in Eq.2 is omitted, and the loss is computed directly in the image space using Eq.7. For each prediction step, active LEGO-conditioning blocks are trained jointly with the shared blocks in both phases.

4.2.2 Chain of Rendering Decomposition (Chord). Multi-modal dense prediction is challenging [Yang et al. 2025]. To simplify the problem, we follow Simchony et al. [Simchony et al. 1990] to integrate height h from the normal map n , reducing the task to four channels: $\{b, n, r, m\}$. With the implicitly shared light assumption, while a naive gradient-based optimization of the loss $\mathcal{L}(\mathcal{R}(\text{MAT}; l); I_{RGB})$ is possible, the problem is severely under-constrained because multiple

parameter combinations can explain the same rendering. This ambiguity persists when training a model to learn an inverse rendering function $\hat{\text{MAT}} = \mathcal{R}^{-1}(I_{\text{RGB}}; l)$.

To address these challenges, our Chord pipeline divides the problem into three sequential steps:

- (1) **Basecolor Prediction:** Conditioning on I_{RGB} , the first step predicts \hat{b} .
- (2) **Normal Prediction:** From \hat{b} , we compute an approximate irradiance map I_{IRR} . The normal map \hat{n} is then predicted by conditioning on both I_{RGB} and I_{IRR} .
- (3) **Roughness & Metalness Prediction:** Given the estimated \hat{b} , \hat{n} , and I_{IRR} , we approximate the optimal roughness and metalness combination image, denoted as I_{RM} . The roughness and metalness $\{\hat{r}, \hat{m}\}$ are predicted by conditioning on both I_{RGB} and I_{RM} .

Basecolor Prediction. We begin by predicting the basecolor to minimize accumulated errors along the chain. As shown in Fig. 2, the data distribution of b is the closest to that of the input RGB images. This makes it easier for the model to learn the transition between the two modalities.

Normal Prediction. In modern PBR workflows, normal maps encode geometric details that are independent of base color variations. Directly conditioning normal prediction on I_{RGB} can introduce noise since color information is largely irrelevant to geometry. Instead, under the assumption of single directional lighting, we compute an approximate irradiance image I_{IRR} by:

$$I_{\text{IRR}} = I_{\text{RGB}}/b \quad (3)$$

This removes color dependence from diffuse shading and preserves lighting and geometric cues in the irradiance. We empirically verify that the error introduced from specular terms is negligible. The resulting I_{IRR} serves as a cleaner conditioning representation for normal prediction, particularly by decoupling diffuse albedo effects.

Roughness & Metalness Prediction. Similar to the motivation of previous steps, we aim to isolate and extract representation closer to the target channels $\{r, m\}$. We first estimate lighting direction \mathbf{l}^* using an energy-decay heuristic on the approximate irradiance image (see Section A.2 of supplementary material). We then perform a grid search to minimize:

$$\text{MSE}(x) = \|\hat{I}_{\mathcal{R}}(x) - I_{\text{RGB}}(x)\|_2^2 \quad (4)$$

where $\hat{I}_{\mathcal{R}}(x) = \mathcal{R}(\hat{b}(x), \hat{n}(x), r(x), m(x); \mathbf{l}^*)$. The discrete search space \mathcal{S} is defined as:

$$\mathcal{S} = \left\{ \left(\frac{25+5i}{255}, j \right) \mid i \in \mathbb{Z}, 0 \leq i \leq 40, j \in \{0, 1\} \right\} \quad (5)$$

yielding 41 roughness values and binary metalness. The optimal per-pixel solution is:

$$I_{\text{RM}}(x) = \begin{bmatrix} r^*(x) \\ m^*(x) \end{bmatrix} = \underset{(r,m) \in \mathcal{S}}{\text{argmin}} \text{MSE}(x) \quad (6)$$

Single-step Phase Loss. We compute loss in image space, by setting $t = T$ and decode latent using VAE decoder, and our loss combines:

$$\begin{aligned} \mathcal{L} = & \underbrace{\|\hat{\text{MAT}} - \text{MAT}\|_1}_{\text{Pixel}} + \underbrace{\|\Phi(\hat{\text{MAT}}) - \Phi(\text{MAT})\|_1}_{\text{Perceptual}} \\ & + \underbrace{\|\mathcal{R}(\hat{\text{MAT}}; l) - \mathcal{R}(\text{MAT}; l)\|_1}_{\text{Render}} \end{aligned} \quad (7)$$

where $\text{MAT} = \{b, n, r, m\}$, $\hat{\text{MAT}}$ are predictions, Φ is pre-trained VGG-16 [Johnson et al. 2016] and l is randomly rotated directional light per iteration. This simplified formulation is for clarity, in the complete loss function, we use cosine similarity for the normal channel \hat{n} instead of the ℓ_1 loss used for other channels:

$$\mathcal{L}_n = 1 - \hat{n} \cdot n \quad (8)$$

This penalizes angular discrepancies and encourages alignment between predicted and ground truth normals. For the render loss, we combine ℓ_1 and VGG perceptual losses. At each iteration, the lighting direction l is randomly sampled 8 times to generate 8 rendered image pairs. A coefficient $\lambda = 0.005$ is applied to the perceptual loss terms during combination. The complete loss is:

$$\begin{aligned} \mathcal{L}_{\text{complete}} = & \|\hat{\text{MAT}} \setminus \hat{n} - \text{MAT} \setminus n\|_1 + \mathcal{L}_n \\ & + \lambda \|\Phi(\hat{\text{MAT}}) - \Phi(\text{MAT})\|_1 \\ & + \|\mathcal{R}(\hat{\text{MAT}}; l) - \mathcal{R}(\text{MAT}; l)\|_1 \\ & + \lambda \|\Phi(\mathcal{R}(\hat{\text{MAT}}; l)) - \Phi(\mathcal{R}(\text{MAT}; l))\|_1. \end{aligned} \quad (9)$$

5 Experiments

5.1 Implementation Details

Our texture RGB generation model is based on SDXL [Podell et al. 2024], fine-tuning it on 1,000 high-quality texture rendering images rendered by \mathcal{R} with descriptive captions.

To train our material estimation model, we constructed a dataset by combining materials from MatSynth and private data, resulting in a total of 28,344 materials after augmentation. During training, each material was resized and randomly cropped to a resolution of 512×512 . For a fair comparison, we retrained several baselines, including SurfaceNet, MatFusion, RGB \rightarrow X, Lotus, and E2E-FT on our dataset. Training details for our method are provided in the supplementary material Section A.1.

5.2 Material Generation

We compare our method with MatFuse [Vecchio et al. 2024b] for conditioned material generation (Fig. 5). While MatFuse directly predicts all four material channels, our two-stage approach generates a texture RGB image first, then decomposes it into channels. Our method significantly outperforms those of MatFuse in terms of both condition alignment and visual quality. See Section 6 for additional material generation applications.

5.3 Material Estimation

We evaluate our method on two datasets: the test split of MatSynth [Vecchio and Deschaintre 2024], containing 89 unique materials, and a curated test set of 250 unique materials from the Substance

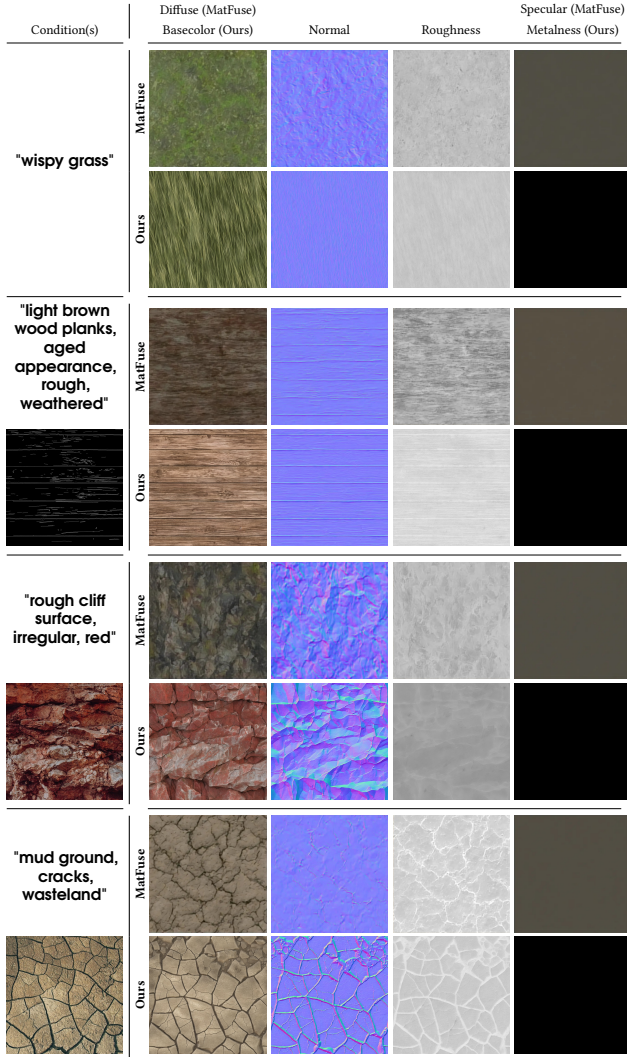


Fig. 5. **Material Generation Comparison with MatFuse** [Vecchio et al. 2024b]. Prompts are prefixed with "A material of" for MatFuse and "texture of" for our method. We compare three conditioning scenarios: text only, text with sketch, and text with reference image. Reference image from Pexels and Pixnio.

Asset Library [Adobe 2024], ensuring no overlap with the training data. The detailed material category distributions are provided in the supplementary material Section A.3. Each material was rendered under four directional lights positioned at the image corners, resulting in 356 and 1,000 evaluation images at a resolution of 1k. Our evaluation encompasses both single-modality estimation, comparing with other dense prediction methods, and full-modalities estimation, compared with other material estimation approaches. We use PSNR and LPIPS to evaluate the similarity between predictions and ground truth (GT) channels.

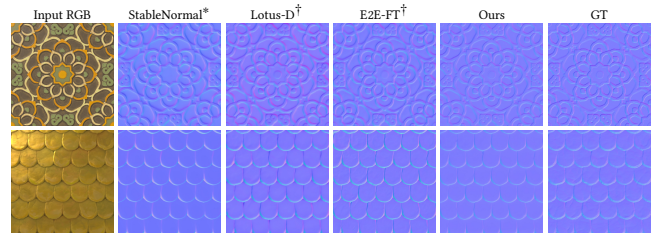


Fig. 6. **Qualitative normal estimation comparisons.**

Table 1. **Normal estimation compared to single-modality methods on Substance test set.** †: trained on our dataset, *: author-provided weights.

Method	PSNR↑	LPIPS↓	Number of Modalities
StableNormal*	20.03	0.502	1
Lotus-D†	22.76	0.371	1
Lotus-G†	22.06	0.416	1
E2E-FT†	24.07	0.379	1
Ours	23.32	0.334	4

Table 2. **Material estimation on MatSynth test split.** †: trained on our dataset, *: author-provided weights.

Method	Basecolor		Normal		Roughness	
	PSNR↑	LPIPS↓	PSNR↑	LPIPS↓	PSNR↑	LPIPS↓
Material Palette*	17.09	0.381	22.78	0.414	15.00	0.593
SurfaceNet†	24.93	0.345	25.45	0.489	16.09	0.605
MatFusion†	24.39	0.377	23.00	0.486	14.59	0.624
RGB→X†	25.79	0.313	25.67	0.361	18.11	0.512
Ours	28.78	0.269	26.65	0.353	19.31	0.532

Method	Metalness		Height		Relit	
	PSNR↑	LPIPS↓	PSNR↑	LPIPS↓	PSNR↑	LPIPS↓
SurfaceNet†	61.16	0.142	17.72	0.534	22.55	0.363
MatFusion†	29.91	0.436	17.52	0.580	22.29	0.382
RGB→X†	61.40	0.102	18.80	0.508	23.24	0.344
Ours	71.93	0.089	19.36	0.467	24.40	0.318

5.3.1 Single-modality Estimation. Different tasks have varying criteria for basecolor, with some PBR materials baking ambient occlusion into the basecolor and others not. Since a certain proportion of materials in our dataset include baked AO, direct comparison with intrinsic decomposition methods [Careaga and Aksoy 2023] is challenging. Therefore, we focus on normal channel estimation. Qualitative results in Fig. 6 and numerical results in Table 1 show that our model remains robust and competitive with state-of-the-art methods, even when predicting four modalities simultaneously.

5.3.2 Full-Modalities Estimation. We compare our method with RGB→X, SurfaceNet, MatFusion, and Material Palette for material estimation. The *Relit* measurements are obtained by rendering the material under nine predefined point lights and directional lights. As shown in Fig. 7, Table 2, Table 3 and Table 4. Our model delivers superior quality while achieving an 11× speedup compared to RGB→X. Additionally, our approach remains robust on unseen generated texture images and in-the-wild photographs, as illustrated in Fig.8

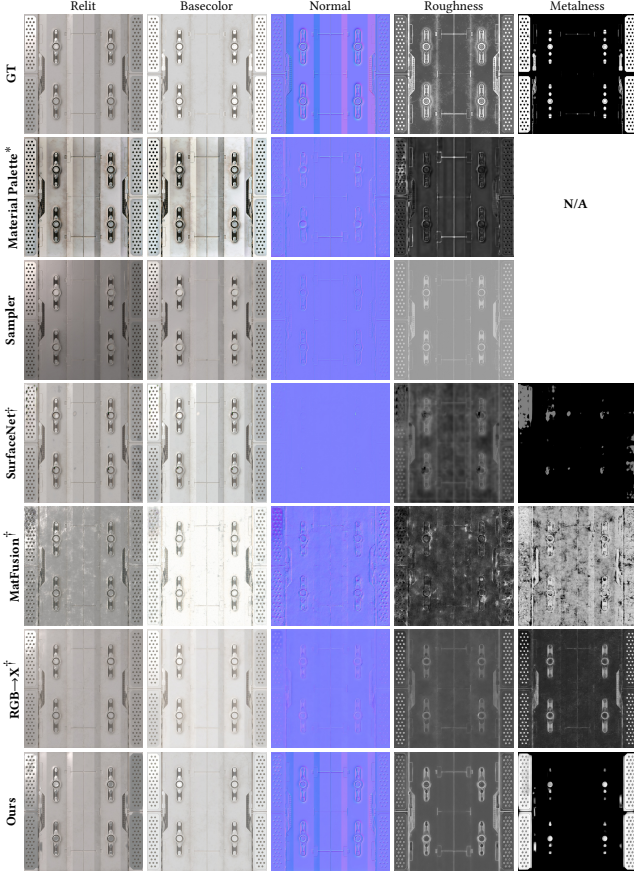


Fig. 7. **Qualitative PBR estimation comparisons.** We also include results from Substance 3D Sampler’s feature called “AI-Powered Image to Material”.

Table 3. **Material estimation on Substance test set.** †: trained on our dataset, *: author-provided weights.

Method	Basecolor		Normal		Roughness	
	PSNR↑	LPIPS↓	PSNR↑	LPIPS↓	PSNR↑	LPIPS↓
Material Palette*	16.04	0.384	19.97	0.417	14.32	0.590
SurfaceNet†	24.60	0.326	21.91	0.508	15.02	0.607
MatFusion†	25.35	0.347	20.69	0.503	14.08	0.622
RGB→X†	25.72	0.317	22.56	0.364	16.72	0.536
Ours	29.05	0.269	23.32	0.334	17.48	0.550

Method	Metalness		Height		Relit	
	PSNR↑	LPIPS↓	PSNR↑	LPIPS↓	PSNR↑	LPIPS↓
SurfaceNet†	64.45	0.118	21.09	0.512	21.54	0.344
MatFusion†	32.66	0.441	20.12	0.526	21.75	0.362
RGB→X†	64.96	0.088	22.64	0.489	21.91	0.340
Ours	77.67	0.064	23.36	0.470	22.94	0.309

and Fig.9. For further visual comparisons with ControlMat [Vecchio et al. 2024a], SurfaceNet [Vecchio et al. 2021], and MaterIA [Martin et al. 2022], please refer to Section A.4.1 of supplementary material.

Table 4. **Inference time for full-modality methods.** Times are measured on an RTX A6000 GPU.

	SurfaceNet	MatFusion	RGB→X	Ours
Time (Seconds)	0.6	46.4	23.6	2.1

5.4 Ablation Study

We validate the components of our pipeline through comprehensive ablation studies. All experiments are initialized using SD 2.1 and fine-tuned on our dataset for 20 epochs, except for the pretrained version of our method, which includes an additional 5 epochs of diffusion pretraining. As presented in Table 5, compared to the baseline (RGB→X), our approach demonstrates that using single-step diffusion with the loss computed directly in image space (+Single-step) improves PSNR but yields worse LPIPS due to blurrier outputs. This issue can be mitigated by incorporating a combined loss (+Combined Loss) described in Eq.9 (excluding the render loss terms), which improves the LPIPS score.

Directly applying a naive chained scheme (+Chain), which uses previous-step predictions as conditioning inputs for the current step, yields only marginal performance improvements. This is primarily due to interference caused by shared model weights across different modalities. By incorporating LEGO-conditioning into the chained pipeline (+LEGO-conditioning), this issue is mitigated through the use of modality-specific weights, leading to more effective multi-channel prediction.

We further evaluate the effect of computing I_{IRR} and I_{RM} , and show that both contribute to improved estimation. Finally, including render loss and Pretraining Phase yields additional performance gains.

6 Applications

In this section, we explore the potential applications of our method. Due to the generate-and-estimate framework, our method inherits the versatility and controllability of the large text-to-image models. Specifically, we leverage tools such as ControlNet [Zhang et al. 2023], IP-Adapter [Ye et al. 2023] and RePaint [Lugmayr et al. 2022] to guide the texture RGB generation process and subsequently estimate SVBRDF channels. Examples can be found in Fig. 8 and Fig. 10.

Text to Material. In this application, users provide a text prompt to guide the generation process. This operates similarly to standard text-to-image methods, with the added stage of material estimation.

Image to Material. Leveraging the image-to-image functionality of the generation stage, users can provide a reference image to guide the generation process. This facilitates applications such as reference-based material synthesis and variation generation.

Structure-controlled Generation. With additional pre-trained ControlNet weights, such as those for line art or depth maps, users can control the generation process to preserve structural layouts specified by the input conditions, enhancing user controllability.

Material Editing. By incorporating an additional in-painting model trained using methods such as RePaint [Lugmayr et al. 2022], users

Table 5. Material estimation ablation study on Substance test set.

Method	Basecolor		Normal		Roughness		Metalness		Height		Relit		Inference (Seconds)	Parameters (B)
	PSNR↑	LPIPS↓	PSNR↑	LPIPS↓	PSNR↑	LPIPS↓	PSNR↑	LPIPS↓	PSNR↑	LPIPS↓	PSNR↑	LPIPS↓		
RGB→X	25.72	0.317	22.56	0.364	16.72	0.536	64.96	0.088	22.64	0.489	21.91	0.340	23.6	1.3
+Single-step	27.95	0.354	23.06	0.400	18.15	0.640	58.86	0.120	23.33	0.479	22.55	0.373	1.9	1.3
+Combined Loss	28.12	0.285	22.96	0.345	18.39	0.566	73.58	0.071	22.95	0.472	22.42	0.315	1.9	1.3
+Chain	28.29	0.284	23.04	0.346	18.24	0.571	73.68	0.083	23.36	0.475	22.50	0.310	1.9	1.3
+LEGO-conditioning	28.45	0.283	23.16	0.343	18.59	0.559	72.08	0.085	22.92	0.474	22.52	0.315	1.9	1.4
+Approx. Irradiance	28.53	0.291	23.25	0.339	18.50	0.576	80.14	0.061	23.54	0.476	22.72	0.316	1.9	1.4
+RM Grid Search	28.39	0.286	23.26	0.340	17.91	0.594	70.02	0.076	23.53	0.471	22.76	0.314	2.1	1.4
+Render Loss (Ours)	28.59	0.283	23.31	0.344	16.97	0.633	78.61	0.077	23.34	0.469	22.88	0.311	2.1	1.4
+Pretraining (Ours)	29.05	0.269	23.32	0.334	17.48	0.550	77.67	0.064	23.36	0.470	22.94	0.309	2.1	1.4

can edit generated materials. For example, they can mask specific areas of the texture RGB and regenerate to modify the material.

7 Discussion and Future Work

Lighting Assumption. Our generate-and-estimate framework assumes generated RGB textures (I_{RGB}) have consistent directional lighting. This usually works but fails for glossy surfaces, leading to less accurate material estimation. The main problem is a conflict: I_{RGB} must be tileable and lit by directional light. Our circular padding makes generated images tileable, but causes edge gradients and highlights of glossy surface to wrap around and bleed across the entire image. This spreads incorrect lighting across the image, creating inconsistencies expected by the material estimation pipeline. In the future, we could generate two images per material: one without tile constraints to capture specular effects, and one tileable for non-specular details, then process them through separate branches.

Baked-in Shadows in Basecolor. Our material estimation results occasionally show baked in shadows in the predicted basecolor channel. We believe this issue arises from the presence of baked ambient occlusion (AO) in many materials within our training dataset. This problem can be reduced by using higher quality material data or by applying shadow removal techniques, such as the method proposed in [Zhao et al. 2025; Zhu et al. 2022], to preprocess our dataset.

Limited Generalization Ability. We employ single-step fine-tuning to train our material estimation model. While this approach yields stronger performance on PBR material test datasets, it can compromise generalization to in-the-wild images (see Fig.9, row 4, basecolor). This limitation could be mitigated in future work by adopting alternative single-step or few-step generative modeling techniques, such as rectified flow [Liu et al. 2022] or mean flow [Geng et al. 2025].

8 Conclusion

In this paper, we introduce a generate-and-estimate framework for material generation. The texture RGB generation stage leverages the capabilities of large text-to-image models to ensure prompt alignment and user control, while maintaining consistent lighting across generated images. In the material estimation stage, we introduce a novel chain-of-rendering-decomposition pipeline that leverages the known lighting assumptions to sequentially estimate SVBRDF modalities. This step-by-step approach integrates PBR cues directly

into the conditioning inputs of the estimation model. Our method significantly outperforms baseline approaches in both user control alignment and output quality, and demonstrates strong versatility across a range of material generation applications.

To the best of our knowledge, this is the first work to introduce chained image-conditional diffusion models with PBR-aware rendering decomposition, offering a practical and effective solution to the inherently under-constrained problem of inverse rendering in material estimation.

Acknowledgments

We thank the anonymous reviewers for their valuable feedback. We are also grateful to Georges Nader, Arnaud Schoentgen, Alexis Rolland, and Yves Jacquier for their helpful discussions and proof-reading. Zhi Ying is grateful for the unwavering family support from Xian Gong and Li Ying. This work was supported by Ubisoft.

References

- Adobe. 2024. *Substance 3D Assets library*. <https://substance3d.adobe.com/assets>
- Miika Aittala, Tim Weyrich, and Jaakko Lehtinen. 2015. Two-shot SVBRDF capture for stationary materials. *ACM Trans. on Graphics* (2015).
- Chris Careaga and Yağız Aksoy. 2023. Intrinsic Image Decomposition via Ordinal Shading. *ACM Trans. on Graphics* 43, 1, Article 12 (2023), 24 pages.
- Chris Careaga and Yağız Aksoy. 2024. Colorful Diffuse Intrinsic Image Decomposition in the Wild. *ACM Trans. on Graphics* 43, 6, Article 178 (2024), 12 pages.
- Dave Zhenyu Chen, Yawar Siddiqui, Hsin-Ying Lee, Sergey Tulyakov, and Matthias Nießner. 2023. Text2tex: Text-driven texture synthesis via diffusion models. In *Proceedings of the IEEE/CVF International Conference on Computer Vision*. 18558–18568.
- R. L. Cook and K. E. Torrance. 1982. A Reflectance Model for Computer Graphics. *ACM Trans. Graph.* 1, 1 (Jan. 1982), 7–24. doi:10.1145/357290.357293
- Valentin Deschaintre, Miika Aittala, Fredo Durand, George Drettakis, and Adrien Bousseau. 2018. Single-image SVBRDF capture with a rendering-aware deep network. *ACM Trans. on Graphics* (2018).
- Xiao Fu, Wei Yin, Mu Hu, Kaixuan Wang, Yuexin Ma, Ping Tan, Shaojie Shen, Dahua Lin, and Xiaoxiao Long. 2024. GeoWizard: Unleashing the Diffusion Priors for 3D Geometry Estimation from a Single Image. In *Eur. Conf. Comput. Vis. (ECCV)*.
- Duan Gao, Xiao Li, Yue Dong, Pieter Peers, Kun Xu, and Xin Tong. 2019. Deep inverse rendering for high-resolution SVBRDF estimation from an arbitrary number of images. *ACM Trans. on Graphics* (2019).
- Gonzalo Martin Garcia, Karim Abou Zeid, Christian Schmidt, Daan de Geus, Alexander Hermans, and Bastian Leibe. 2024. Fine-tuning image-conditional diffusion models is easier than you think. *arXiv preprint arXiv:2409.11355* (2024).
- Zhengyang Geng, Mingyang Deng, Xingjian Bai, J Zico Kolter, and Kaiming He. 2025. Mean flows for one-step generative modeling. *arXiv preprint arXiv:2505.13447* (2025).
- Paul Guerrero, Miloš Hašan, Kalyan Sunkavalli, Radomír Měch, Tamy Boubekeur, and Niloy J. Mitra. 2022. MatFormer: a generative model for procedural materials. *ACM Trans. on Graphics* (2022).
- Yu Guo, Cameron Smith, Miloš Hašan, Kalyan Sunkavalli, and Shuang Zhao. 2020. MaterialGAN: reflectance capture using a generative SVBRDF model. *ACM Trans.*

- on Graphics (2020).
- Jing He, Haodong Li, Wei Yin, Yixun Liang, Leheng Li, Kaiqiang Zhou, Hongbo Liu, Bingbing Liu, and Ying-Cong Chen. 2024. Lotus: Diffusion-based Visual Foundation Model for High-quality Dense Prediction. *arXiv:2409.18124* (2024).
- Zhen He, Jie Guo, Yan Zhang, Qinghao Tu, Mufan Chen, Yanwen Guo, Pengyu Wang, and Wei Dai. 2023. Text2Mat: Generating Materials from Text. In *Pacific Graphics Short Papers and Posters*.
- Philipp Henzler, Valentin Deschaintre, Niloy J Mitra, and Tobias Ritschel. 2021. Generative Modelling of BRDF Textures from Flash Images. *ACM Trans. on Graphics* (2021).
- Jonathan Ho, Ajay Jain, and Pieter Abbeel. 2020. Denoising Diffusion Probabilistic Models. In *Adv. Neural Inform. Process. Syst. (NeurIPS)*.
- Yijia Hong, Yuan-Chen Guo, Ran Yi, Yulong Chen, Yan-Pei Cao, and Lizhuang Ma. 2024. SuperMat: Physically Consistent PBR Material Estimation at Interactive Rates. *arXiv preprint arXiv:2411.17515* (2024).
- Justin Johnson, Alexandre Alahi, and Li Fei-Fei. 2016. Perceptual losses for real-time style transfer and super-resolution. In *Computer Vision—ECCV 2016: 14th European Conference, Amsterdam, The Netherlands, October 11–14, 2016, Proceedings, Part II 14*. Springer, 694–711.
- Brian Karis. 2013. Real shading in unreal engine 4. *Proc. Physically Based Shading Theory Practice* 4, 3 (2013), 1.
- Bingxin Ke, Anton Obukhov, Shengyu Huang, Nando Metzger, Rodrigo Caye Daudt, and Konrad Schindler. 2024. Repurposing Diffusion-Based Image Generators for Monocular Depth Estimation. In *IEEE Conf. Comput. Vis. Pattern Recog. (CVPR)*.
- Peter Kocsis, Vincent Sitzmann, and Matthias Nießner. 2024. Intrinsic Image Diffusion for Indoor Single-view Material Estimation. In *IEEE Conf. Comput. Vis. Pattern Recog. (CVPR)*.
- Hsin-Ying Lee, Hung-Yu Tseng, Hsin-Ying Lee, and Ming-Hsuan Yang. 2024. Exploiting Diffusion Prior for Generalizable Dense Prediction. In *IEEE Conf. Comput. Vis. Pattern Recog. (CVPR)*.
- Xiao Li, Yue Dong, Pieter Peers, and Xin Tong. 2017. Modeling surface appearance from a single photograph using self-augmented convolutional neural networks. *ACM Trans. on Graphics* (2017).
- Zhengqin Li, Kalyan Sunkavalli, and Manmohan Chandraker. 2018. Materials for Masses: SVBRDF Acquisition with a Single Mobile Phone Image. In *Eur. Conf. Comput. Vis. (ECCV)*.
- Xingchao Liu, Chengyue Gong, and Qiang Liu. 2022. Flow straight and fast: Learning to generate and transfer data with rectified flow. *arXiv preprint arXiv:2209.03003* (2022).
- Xian Liu, Jian Ren, Aliaksandr Siarohin, Ivan Skorokhodov, Yanyu Li, Dahua Lin, Xihui Liu, Ziwei Liu, and Sergey Tulyakov. 2023. Hyperhuman: Hyper-realistic human generation with latent structural diffusion. *arXiv preprint arXiv:2310.08579* (2023).
- Ivan Lopes, Fabio Pizzati, and Raoul de Charette. 2024. Material Palette: Extraction of Materials from a Single Image. In *IEEE Conf. Comput. Vis. Pattern Recog. (CVPR)*.
- Andreas Lugmayr, Martin Danelljan, Andres Romero, Fisher Yu, Radu Timofte, and Luc Van Gool. 2022. Repaint: Inpainting using denoising diffusion probabilistic models. In *Proceedings of the IEEE/CVF conference on computer vision and pattern recognition*. 11461–11471.
- Xiaohe Ma, Valentin Deschaintre, Miloš Hašan, Fujun Luan, Kun Zhou, Hongzhi Wu, and Yiwei Hu. 2025. MaterialPicker: Multi-Modal DiT-Based Material Generation. *ACM Transactions on Graphics (TOG)* 44, 4 (2025), 1–12.
- Rosalie Martin, Arthur Roullier, Romain Rouffet, Adrien Kaiser, and Tamy Boubekeur. 2022. MaterIA: Single Image High-Resolution Material Capture in the Wild. *Comput. Graph. Forum* (2022).
- Jaakko Lehtinen, Miika Aittala, Timo Aila. 2016. Reflectance modeling by neural texture synthesis. *ACM Trans. on Graphics* (2016).
- Dustin Podell, Zion English, Kyle Lacey, Andreas Blattmann, Tim Dockhorn, Jonas Müller, Joe Penna, and Robin Rombach. 2024. SDXL: Improving Latent Diffusion Models for High-Resolution Image Synthesis. In *The Twelfth International Conference on Learning Representations*. <https://openreview.net/forum?id=di5ZzR8xgf>
- Robin Rombach, Andreas Blattmann, Dominik Lorenz, Patrick Esser, and Björn Ommer. 2021. High-Resolution Image Synthesis with Latent Diffusion Models. In *IEEE Conf. Comput. Vis. Pattern Recog. (CVPR)*.
- Olaf Ronneberger, Philipp Fischer, and Thomas Brox. 2015. U-Net: Convolutional Networks for Biomedical Image Segmentation. In *Medical Image Computing and Computer-Assisted Intervention*. Springer International Publishing.
- Tim Salimans and Jonathan Ho. 2022. Progressive Distillation for Fast Sampling of Diffusion Models. In *Int. Conf. Learn. Represent. (ICLR)*. <https://openreview.net/forum?id=TLdXlpzh0l>
- Sam Sartor and Pieter Peers. 2023. Matfusion: a generative diffusion model for svbrdf capture. In *SIGGRAPH Asia 2023 conference papers*. 1–10.
- Christophe Schlick. 1994. An inexpensive BRDF model for physically-based rendering. In *Computer graphics forum*, Vol. 13. Wiley Online Library, 233–246.
- Liang Shi, Beichen Li, Miloš Hašan, Kalyan Sunkavalli, Tamy Boubekeur, Radomir Mech, and Wojciech Matusik. 2020. MATch: differentiable material graphs for procedural material capture. *ACM Trans. on Graphics* (2020).
- Tal Simchony, Rama Chellappa, and Min Shao. 1990. Direct analytical methods for solving Poisson equations in computer vision problems. *IEEE transactions on pattern analysis and machine intelligence* 12, 5 (1990), 435–446.
- Yang Song, Jascha Sohl-Dickstein, Diederik P. Kingma, Abhishek Kumar, Stefano Ermon, and Ben Poole. 2021. Score-Based Generative Modeling through Stochastic Differential Equations. In *Int. Conf. Learn. Represent. (ICLR)*.
- TS Trowbridge and Karl P Reitz. 1975. Average irregularity representation of a rough surface for ray reflection. *JOSA* 65, 5 (1975), 531–536.
- Giuseppe Vecchio and Valentin Deschaintre. 2024. MatSynth: A Modern PBR Materials Dataset. In *IEEE Conf. Comput. Vis. Pattern Recog. (CVPR)*.
- Giuseppe Vecchio, Rosalie Martin, Arthur Roullier, Adrien Kaiser, Romain Rouffet, Valentin Deschaintre, and Tamy Boubekeur. 2024a. Controlmat: a controlled generative approach to material capture. *ACM Transactions on Graphics* 43, 5 (2024), 1–17.
- Giuseppe Vecchio, Simone Palazzo, and Concetto Spampinato. 2021. SurfaceNet: Adversarial SVBRDF Estimation from a Single Image. In *Int. Conf. Comput. Vis. (ICCV)*.
- Giuseppe Vecchio, Renato Sortino, Simone Palazzo, and Concetto Spampinato. 2024b. MatFuse: Controllable Material Generation with Diffusion Models. *IEEE Conf. Comput. Vis. Pattern Recog. (CVPR)* (2024).
- Li-Yi Wei, Sylvain Lefebvre, Vivek Kwatra, and Greg Turk. 2009. State of the art in example-based texture synthesis. *Eurographics 2009, State of the Art Report, EG-STAR* (2009), 93–117.
- Linxuan Xin, Zheng Zhang, Jinfu Wei, Wei Gao, and Duan Gao. 2024. DreamPBR: Text-driven Generation of High-resolution SVBRDF with Multi-modal Guidance. *arXiv:2404.14676* (2024).
- Guangkai Xu, Yongtao Ge, Mingyu Liu, Chengxiang Fan, Kangyang Xie, Zhiyue Zhao, Hao Chen, and Chunhua Shen. 2024. Diffusion Models Trained with Large Data Are Transferable Visual Models. *arXiv:2403.06090* (2024).
- Bowen Xue, Claudio Guarnera, Shuang Zhao, and Zahra Montazeri. 2024. Reflectance-Fusion: Diffusion-based text to SVBRDF Generation. In *Eurographics Symposium on Rendering*. Eurographics Association.
- Yuqi Yang, Peng-Tao Jiang, Qibin Hou, Hao Zhang, Jinwei Chen, and Bo Li. 2025. Multi-Task Dense Predictions via Unleashing the Power of Diffusion. In *The Thirteenth International Conference on Learning Representations*. <https://openreview.net/forum?id=TzdTRC85SQ>
- Hu Ye, Jun Zhang, Sibao Liu, Xiao Han, and Wei Yang. 2023. IP-Adapter: Text Compatible Image Prompt Adapter for Text-to-Image Diffusion Models. (2023).
- Liang Yuan, Dingkun Yan, Suguru Saito, and Issei Fujishiro. 2024. DiffMat: Latent diffusion models for image-guided material generation. *Visual Informatics* (2024).
- Zheng Zeng, Valentin Deschaintre, Iliyan Georgiev, Yannick Hold-Geoffroy, Yiwei Hu, Fujun Luan, Ling-Qi Yan, and Miloš Hašan. 2024. RGB \leftrightarrow X: Image decomposition and synthesis using material- and lighting-aware diffusion models. *ACM Trans. on Graphics* (2024).
- Lvmin Zhang, Anyi Rao, and Maneesh Agrawala. 2023. Adding conditional control to text-to-image diffusion models. In *Proceedings of the IEEE/CVF International Conference on Computer Vision*. 3836–3847.
- Yezi Zhao, Beibei Wang, Yanning Xu, Zheng Zeng, Lu Wang, and Nicolas Holzschuch. 2020. Joint SVBRDF Recovery and Synthesis From a Single Image using an Unsupervised Generative Adversarial Network. In *Eurographics Symposium on Rendering*.
- Zibo Zhao, Zeqiang Lai, Qingxiang Lin, Yunfei Zhao, Haolin Liu, Shuhui Yang, Yifei Feng, Mingxin Yang, Sheng Zhang, Xianghui Yang, et al. 2025. Hunyuan3d 2.0: Scaling diffusion models for high resolution textured 3d assets generation. *arXiv preprint arXiv:2501.12202* (2025).
- Xilong Zhou, Milos Hasan, Valentin Deschaintre, Paul Guerrero, Kalyan Sunkavalli, and Nima Khademi Kalantari. 2022. TileGen: Tileable, Controllable Material Generation and Capture. (2022).
- Xilong Zhou, Miloš Hašan, and Valentin Deschaintre. 2023. PhotoMat: A Material Generator Learned from Single Flash Photos. *ACM Trans. on Graphics* (2023).
- Xilong Zhou and Nima Khademi Kalantari. 2022. Look-Ahead Training with Learned Reflectance Loss for Single-Image SVBRDF Estimation. *ACM Trans. on Graphics* (2022).
- Yurui Zhu, Jie Huang, Xueyang Fu, Feng Zhao, Qibin Sun, and Zheng-Jun Zha. 2022. Bijective mapping network for shadow removal. In *Proceedings of the IEEE/CVF Conference on Computer Vision and Pattern Recognition*. 5627–5636.

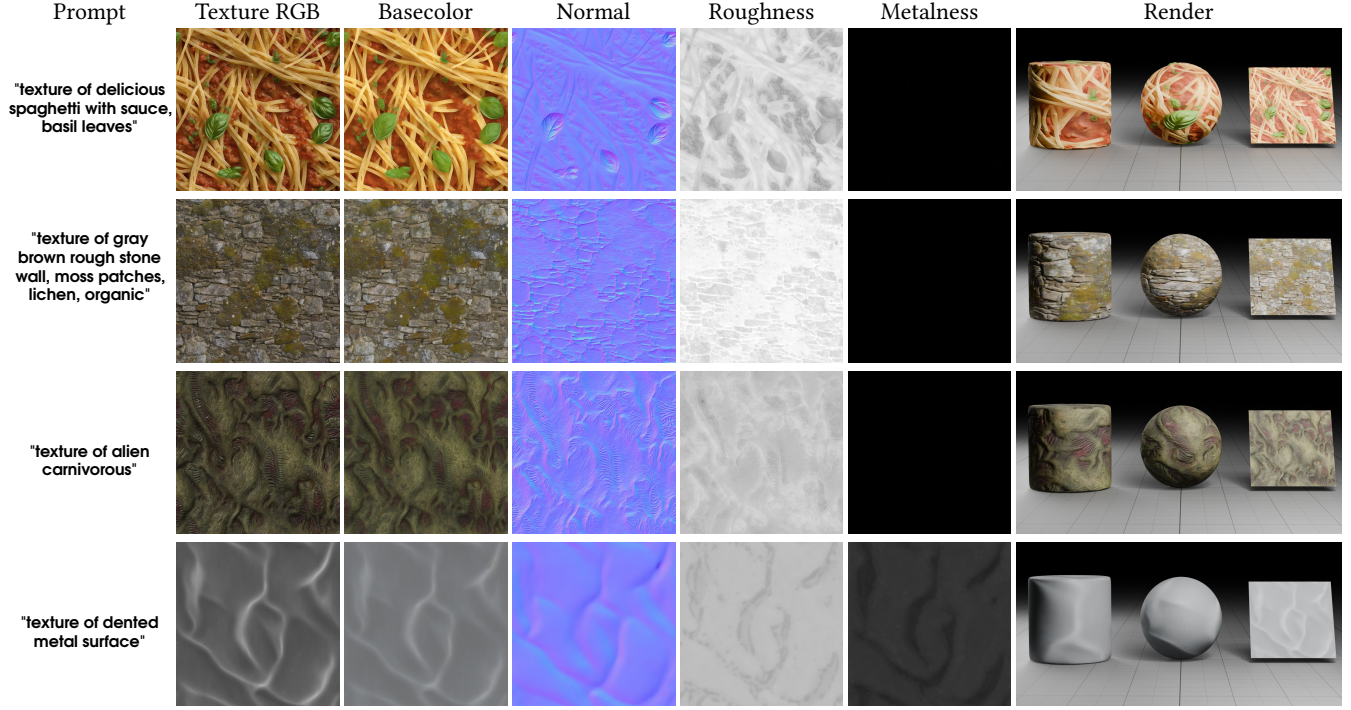


Fig. 8. **PBR material generated by our method.** *Texture RGB* represents I_{RGB} generated by texture generation stage, while *Render* represents re-rendered image from estimated material.

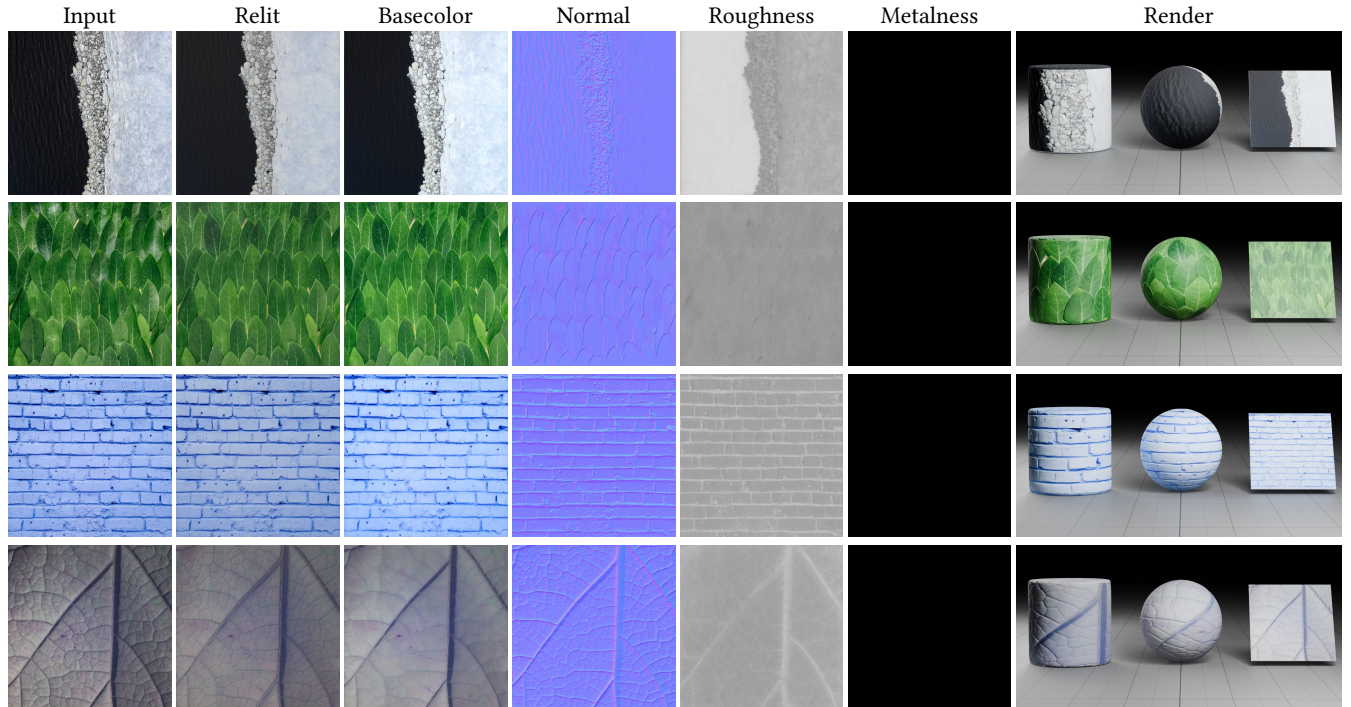
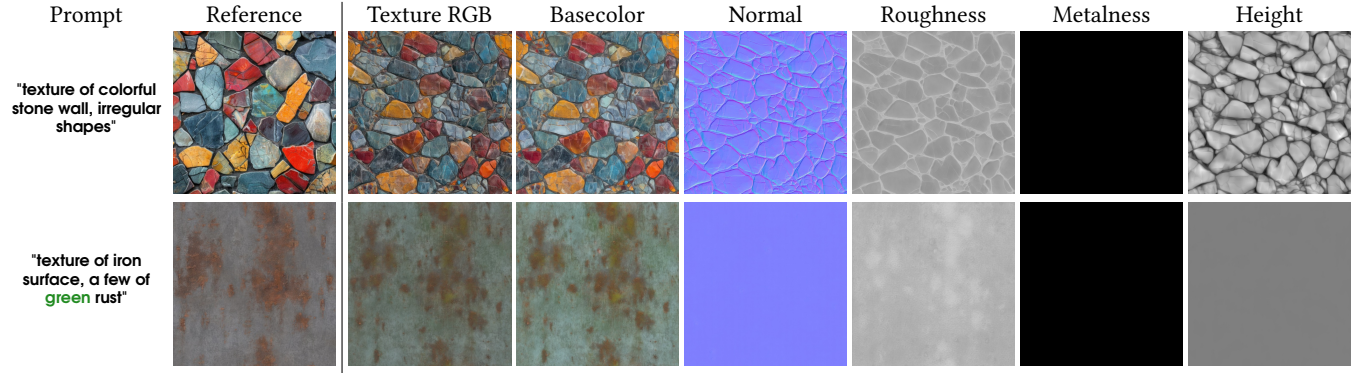
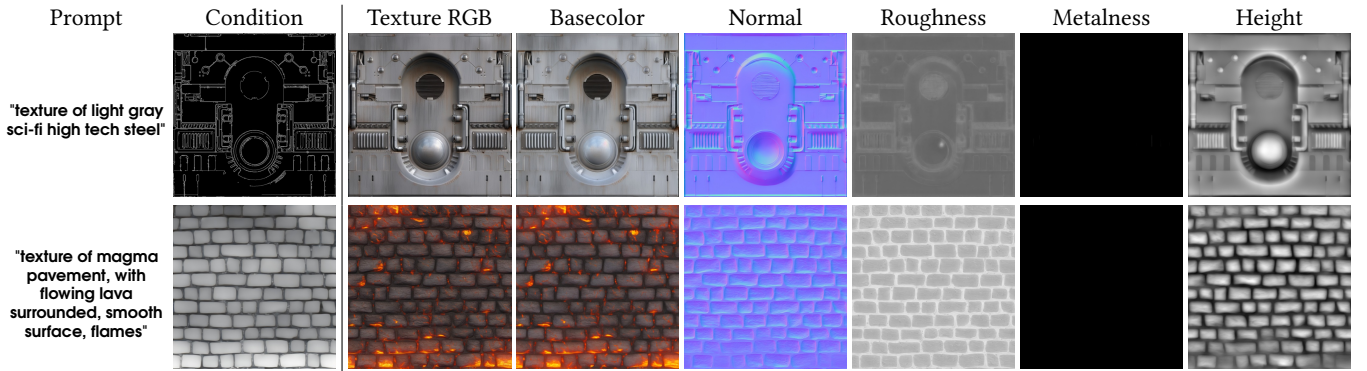


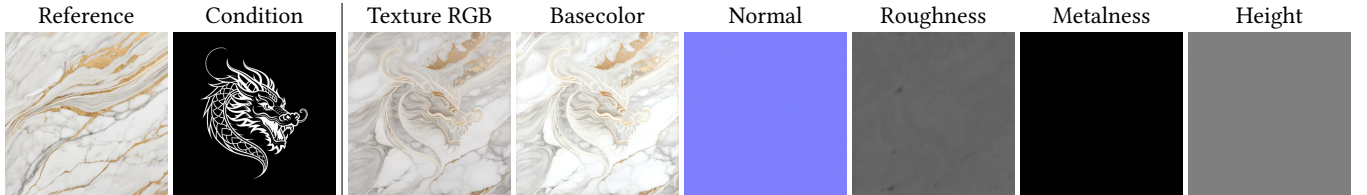
Fig. 9. **Material estimation from in-the-wild photographs.** We demonstrate the robustness of our Chord pipeline using real-world top-down photographs as inputs. Photo from Unsplash.



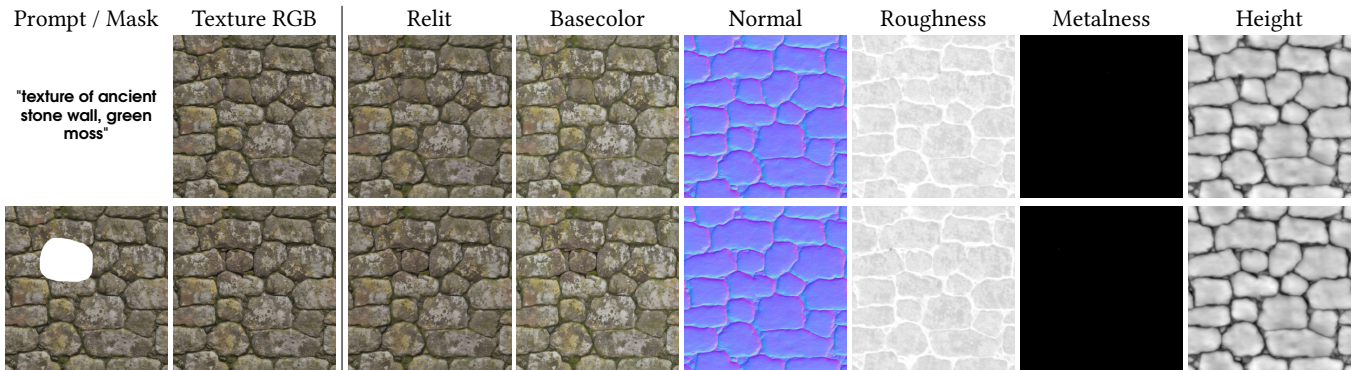
(a) **Image to Material.** Given a reference image, which may be non-tillable, our method generates tillable materials or material variations guided by the corresponding text prompt. Colorful stone reference image from Vecteezy



(b) **Structure-controlled Generation** We present two examples: one using line art as control and the other using depth map as control.



(c) This example illustrates how line art structure guidance is integrated with a reference image during generation.



(d) **Material Editing.** We demonstrate how in-painting can be used to regenerate a masked region in I_{RGB} , resulting in corresponding edits to the estimated material. The material estimation results outside the masked region remain unchanged.

Fig. 10. More applications.